Antonia, R. A.; Tang, S. L.; Djenidi, L.; Danaila, L "Boundedness of the velocity derivative skewness in various turbulent flows". Published in Journal of Fluid Mechanics Vol. 781, p. 727-744 (2015)

Available from: http://dx.doi.org/10.1017/jfm.2015.539

Boundedness of the velocity derivative skewness in various turbulent flows

R. A. Antonia[1], S. L. Tang[1,2], L. Djenidi[1] †, and L. Danaila[3]

[1]School of Engineering, University of Newcastle, NSW 2308, Australia

[2]Institute for Turbulence-Noise-Vibration Interaction and Control, Shenzhen Graduate School, Harbin Institute of Technology, Shenzhen, 518055, P. R. China

[3]CORIA CNRS UMR 6614, Université de Rouen, 76801 Saint Etienne du Rouvray, France

(Received ?; revised ?; accepted ?. - To be entered by editorial office)

The variation of S, the velocity derivative skewness, with the Taylor microscale Reynolds number R_λ is examined for different turbulent flows by considering the locally isotropic form of the transport equation for the mean energy dissipation rate $\overline{\epsilon}_{iso}$. In each flow, the equation can be expressed in the form $S + 2G/R_\lambda = C/R_\lambda$, where G is a non-dimensional rate of destruction of $\overline{\epsilon}_{iso}$ and C is a flow dependent constant. Since $2G/R_\lambda$ is found to be very nearly constant for $R_\lambda \geqslant 70$, S should approach a universal constant when R_λ is sufficiently large, but the way this constant is approached is flow dependent. For example, the approach is slow in grid turbulence and rapid along the axis of a round jet. For all the flows considered, the approach is reasonably well supported by experimental and numerical data. The constancy of S at large R_λ has obvious ramifications for small scale turbulence research since it violates the modified similarity hypothesis introduced by Kolmogorov (1962) but is consistent with the original similarity hypothesis (Kolmogorov 1941a).

1. Introduction

The skewness S of the longitudinal velocity derivative, usually defined as

$$S = \frac{\overline{(\partial u/\partial x)^3}}{\overline{(\partial u/\partial x)^2}^{3/2}} \tag{1.1}$$

(u is the longitudinal velocity fluctuation, x is in the flow direction; the overbar denotes time averaging for experimental data and space/time averaging for numerical data), is an important quantity in turbulent research since it is closely linked to the production of the mean enstrophy or mean energy dissipation rate due to vortex stretching. In particular, the variation of S with the Taylor microscale Reynolds number $R_\lambda (=u'\lambda/\nu$, where λ is the longitudinal Taylor microscale $u'/(\partial u/\partial x)'$ and ν is the kinematic viscosity of the fluid, a prime denotes a r.m.s value) has received a great deal of attention following Kolmogorov's (Kolmogorov 1962) third hypothesis. The majority of the observations and predictions have tended to indicate a slow, though continuous increase of $|S|$ with R_λ, viz.

$$|S| \sim R_\lambda^\alpha \qquad (\alpha > 0) \tag{1.2}$$

when atmospheric surface layer data are included, e.g. Wyngaard & Tennekes (1970); Gibson *et al.* (1970); Champagne *et al.* (1977); Van Atta & Antonia (1980); Sreenivasan & Antonia (1997). However, when the latter data are disregarded (a major reason for doing so is

† Email address for correspondence: lyazid.djenidi@newcastle.edu.au

that these data were obtained at a relatively small height above the ground or ocean surface), the bulk of the laboratory data (e.g. Fig. 5 of Sreenivasan & Antonia (1997)) does not exclude the possibility that -S becomes constant when R_λ approaches 10^3. Since the laboratory data have been collected from a wide range of different flows, $|S|$ may be flow dependent, a possibility that has not been formally acknowledged in the past. How and whether S becomes constant at sufficiently large R_λ should be of special interest to both the engineering and physics turbulence communities. S plays an important role in turbulence modelling, and in particular in the $k-\epsilon$ model where it is involved in the transport equation of $\overline{\epsilon}$, the mean turbulent energy dissipation rate. One consequence of Kolmogorov (1962) (hereafter $K62$) is that $|S|$ continues to increase with R_λ whereas the earlier phenomenology of Kolmogorov (1941a), widely known as $K41$, predicts that all normalized velocity derivative moments should remain constant with R_λ, provided the latter is sufficiently large. Note that the constancy of S at sufficiently large R_λ was underlined by Batchelor (1953).

It should be recognized from the outset that the finite Reynolds number effect (e.g. Qian 1999; Danaila *et al.* 1999; Lindborg 1999) cannot be ignored when $R_\lambda \leqslant 10^3$. As an example, the non-stationarity in the Karman-Howarth (K-H) equation (Karman & Howarth 1938), neglected by Kolmogorov (1941b) and Frisch (1995), needs to be retained to account for this effect. Indeed, Antonia & Burattini (2006) showed that Kolmogorov's 4/5 law is approached more rapidly for forced than decaying turbulence and that the nature of the forcing also matters. The retention of the non-stationarity in the K-H equation, strictly valid for homogeneous and isotropic turbulence, essentially accounts for the inhomogeneity of the large scales and hence the physical processes associated with the initial injection of energy into the flow and its subsequent distribution among the different scales. This virtually ensures that the small scale motion (SSM) will exhibit non-universal features at finite Reynolds numbers, i.e. a dependence on initial and boundary conditions and on the individual nature of the flows. Whereas Antonia & Burattini (2006) focused on inertial range scales, we concentrate here on the limiting behaviour as the scale goes to zero, of the generalized form of the K-H equation, or equivalently the transport equation for $\overline{(\delta q)^2}$ $(=\overline{(\delta u)^2}+\overline{(\delta v)^2}+\overline{(\delta w)^2})$, the velocity increment $\delta\alpha = \alpha(x+r) - \alpha(x)$ between two points separated by a distance r along x, the flow direction; α stands for either u, v, or w, v and w being velocity fluctuations in the y and z directions respectively. The transport equation for $\overline{\epsilon}$ represents an important constraint on how S varies in different flows. Although local isotropy is assumed, we will show that differences in large scale inhomogeneities between different flows result in a non-universal approach of -S towards a constant value as R_λ increases. The different flows we consider are stationary forced periodic box turbulence (or SFPBT), decaying grid turbulence, and the flow along the axis in the self-preserving region of a circular jet. In each case, local isotropy is expected to be reasonably satisfied.

2. Theoretical considerations

An appropriate starting point for our analysis is the transport equation for $\overline{(\delta q)^2}$ in flows or flow regions where departures from local isotropy are small, viz.

$$-\overline{\delta u(\delta q)^2} + 2\nu\frac{\partial}{\partial r}\overline{(\delta q)^2} + I_q = \frac{4}{3}\overline{\epsilon}r. \tag{2.1}$$

The first and second terms on the left side of (2.1) represent the energy transfer and viscous diffusion of energy, respectively. The third term accounts for the inhomogeneity or non-stationarity associated with the large scales. $\overline{\epsilon}$ is defined by

$$\overline{\epsilon} = \nu \overline{\left(\frac{\partial u_i}{\partial x_j} + \frac{\partial u_j}{\partial x_i} \right) \frac{\partial u_j}{\partial x_i}} \qquad (i, j = 1, 2, 3) \tag{2.2}$$

where u_i are the velocity fluctuations in the x_i directions and the double indices convention applies. In the framework of Kolmogorov (1941a), I_q is set to zero, thus ensuring universality. Clearly, any departure from universality will arise from the term I_q which must be retained if turbulence is to be described accurately at all scales. At large r, (2.1) reduces to the one-point energy budget equation whereas in the limit $r \to 0$, (and after some manipulations detailed in Antonia *et al.* (2000)), it reduces to the one-point transport equation of $\overline{\epsilon}$.

For decaying grid turbulence, I_q reflects the streamwise decay of turbulent energy, viz.

$$I_q(r) = -\frac{U}{r^2} \int_0^r s^2 \frac{\partial \overline{(\delta q(s))^2}}{\partial x} ds, \tag{2.3}$$

where the mean velocity U is constant. When $r \to 0$, and assuming isotropy, the transport equation for $\overline{\epsilon}$ simplifies to the equation first considered in detail by Batchelor & Townsend (1947)

$$-U \frac{\partial \overline{\epsilon}_{iso}}{\partial x} = \frac{7}{3\sqrt{15}} \frac{\overline{\epsilon}_{iso}{}^{3/2}}{\nu^{1/2}} \left[S + 2\frac{G}{R_\lambda} \right], \tag{2.4}$$

where

$$G = \overline{u^2} \frac{\overline{(\partial^2 u/\partial x^2)^2}}{\overline{(\partial u/\partial x)^2}^2} \tag{2.5}$$

can be thought of as a destruction coefficient of $\overline{\epsilon}_{iso}$, the isotropic mean energy dissipation rate. Equation (2.4) can be recast in the form (see for example Thiesset *et al.* (2014))

$$S + 2\frac{G}{R_\lambda} = \frac{C}{R_\lambda}, \tag{2.6}$$

where

$$C = \frac{90}{7(1+2R)} \frac{n+1}{n} \tag{2.7}$$

(n is the power-law decay exponent of the longitudinal velocity variance, viz. $\overline{u^2} \sim x^{-n}$, and $R = \overline{v^2}/\overline{u^2}$) is constant if n is constant.

As noted in the introduction, the possible flow dependence of C is of importance both in terms of turbulence modelling and also when testing for the so-called small-scale or internal intermittency effects, first introduced by $K62$. In the former case and the specific context of the $k-\epsilon$ model, the value of C determines the constant in the model. It is now well accepted that the concept of a universal constant is not tenable (see for example George *et al.* (2001)). In the latter case, it seems likely-as will be seen later in this section-that for the same (finite) value of R_λ, the value C may differ in different flows. This in turn implies that the value of S may differ, for nominally the same value of R_λ, in different flows, thus leading to an ambiguity when testing for the effect of intermittency on different small-scale statistics.

With respect to (2.7), it is evident that a large family of curves can be plotted for $S + 2G/R_\lambda$ as a function of R_λ in grid turbulence given the scatter in the magnitude of n that exists in the literature (e.g. George 1992). A power-law decay is tenable strictly when R_λ is constant which corresponds to self-preservation at all scales ($n = 1$, *e.g.*

Meldi & Sagaut (2013) and Djenidi & Antonia (2015)). For most experiments, the power-law decay is only approximate and R_λ continues to decrease with x during the decay. It is worth recalling here Speziale and Bernard's argument (Speziale & Bernard 1992) that $n = 1$ is "the asymptotic state toward which a self-preserving isotropic turbulence is driven at high Reynolds numbers in order to resolve the fundamental imbalance between vortex stretching and viscous diffusion. In the process of resolving this imbalance, compatibility with Kolmogorov scaling is achieved for the small-scale correlations."

On the other hand, there are flow regions e.g. along the axis in the far field of an axisymmetric jet and the far plane wake where self-preservation is satisfied. Provided the initial Reynolds number (based on the jet diameter D and jet velocity U_j or the cylinder diameter d and free stream velocity U_∞) is sufficiently large, there will be a range of x/D or x/d over which R_λ is constant, thus removing any ambiguity when plotting $S + 2G/R_\lambda$ versus R_λ. Since self-preservation is valid, S and $2G/R_\lambda$ do not vary with x. The consequence of self-preservation on various turbulence statistics in these two flow regions have been explored in some detail (Thiesset *et al.* (2014) for axis of axisymmetric jet and Tang *et al.* (2015a) far plane wake). Here we only briefly recall the main steps obtained in Thiesset *et al.* (2014) which lead to the expression for $S + 2G/R_\lambda$.

Along the axis of a round jet, the inhomogeneous term in (2.1) is

$$\begin{aligned} I_q(r) = & -\tfrac{U}{r^2}\int_0^r s^2 \tfrac{\partial \overline{(\delta q(s))^2}}{\partial x} ds \\ & -\tfrac{2}{r^2}\tfrac{dU}{dx}\int_0^r s^2[\overline{(\delta u(s))^2} - \overline{(\delta v(s))^2}] ds. \end{aligned} \tag{2.8}$$

At large r, (2.1) reduces to the one-point energy budget, viz.

$$-\frac{U}{2}\frac{d\overline{q^2}}{dx} - (\overline{u^2} - \overline{v^2})\frac{dU}{dx} = \overline{\epsilon}, \tag{2.9}$$

since the 1st and 2nd terms of the left side of (2.1) become zero when r is large. In contrast to grid turbulence, the mean velocity U ($\sim x^{-1}$) decays with x. Equation (2.9) reflects the balance between $\overline{\epsilon}$ and the sum of the advection and production of the turbulent energy, the latter arising through the interaction between the normal Reynolds stresses and the mean strain rate $\partial U/\partial x$. The jet axis region satisfies self-preservation exactly for $x/D \gtrsim 50$, since R_λ does not vary with x in this region (Burattini *et al.* 2005). The limiting form of (2.1) as $r \to 0$ can be simplified using axisymmetry ($\overline{w^2} = \overline{v^2}$) and local isotropy (Thiesset *et al.* 2014)). The final expression is identical to (2.6), except that C is now given by

$$C = \frac{90}{7(2+R)}. \tag{2.10}$$

Since all the flows mentioned above are of the "decaying" type, it seems appropriate to consider "forced" turbulence flows which are in general less affected by finite Reynolds number or FRN effects (e.g. Antonia & Burattini 2006) than decaying flows. We start by writing Eq. (2.6) in a generalized form

$$S + 2\frac{G}{R_\lambda} = \mathcal{D}, \tag{2.11}$$

where $\mathcal{D}$ is exactly given by

$$\mathcal{D} = \frac{\lim_{r\to 0}\frac{LS(r)}{r^2}}{\overline{\left(\frac{\partial u}{\partial x}\right)^2}^{3/2}}, \tag{2.12}$$

where the term $LS(r)$ reflects the large-scale effects. Its particular form in isotropic decaying turbulence is

$$LS_{decay}(r) = U\frac{\partial\overline{(\delta q)^2}}{\partial x}, \tag{2.13}$$

or, in forced turbulence,

$$LS_{forced}(r) = \overline{\delta u_i \delta u_j}\frac{\partial U_i}{\partial x_j}. \tag{2.14}$$

Term $\mathcal{D}$ may further be written in the form

$$\mathcal{D} = \frac{\lim_{r\to 0}\frac{LS(r)}{r^2}}{\lim_{r\to 0}\frac{1}{r^3}\overline{(\delta u)^2}^{3/2}} \equiv \lim_{r\to 0}\left[r\frac{LS(r)}{\overline{(\delta u)^2}^{3/2}}\right]. \tag{2.15}$$

For decaying turbulence, and considering the expression of the large-scale term $LS \propto \frac{u'}{L}\overline{(\delta u)^2}$, together with

$$\lim_{r\to 0}\frac{\overline{(\delta u)^2}^{1/2}}{r} = \frac{u_K}{\eta} \equiv \frac{u'}{\lambda}, \tag{2.16}$$

term $\mathcal{D}$ becomes

$$\mathcal{D}_{decay} = \frac{u'}{L}/\frac{u'}{\lambda} \propto \frac{\lambda}{L} \propto \frac{1}{R_\lambda}. \tag{2.17}$$

Here, $u_K = (\nu\overline{\epsilon})^{1/4}$ and $\eta = (\nu^3/\overline{\epsilon})^{1/4}$ are the Kolmogorov scales. This demonstration *a priori* circumvents the explicit dependence of the constant C on the decaying exponent n (Eq. (2.7)), which actually depends on R_λ for FRN.

Note here that a similar development holds for the case when several large-scale effects coexist, such as production (due to mean velocity gradients, or coherent motion strain), turbulent diffusion, decay etc. This can be the case of non-equilibrium flows. In these cases also, the final result is that the sum of all large-scale effects behaves as $\propto \frac{1}{R_\lambda}$ for sufficiently high Reynolds numbers.

For forced turbulence, two cases will be considered.

First, an experimental box turbulence produced by pairs of opposed streams that point towards the central area of the flow. Shear turbulence, characterized by $\frac{\partial U_i}{\partial x_j}$ with $i \neq j$ is at this point excluded, because it is characterized by small-scale anisotropy, which is not compatible with the locally isotropic context of this derivation. Therefore, the box turbulence will be characterized by mean velocity gradients along the directions of the mean streams themselves, e.g. $\frac{\partial U}{\partial x} \propto \frac{u'}{L}$, where L is the scale over which the mean stream is stopped, or the scale at which the kinetic energy is injected. The large-scale term becomes

$$LS_{forced}(r) \sim \overline{(\delta u)^2}\frac{dU}{dx}, \tag{2.18}$$

and with a similar development as above, term $\mathcal{D}_{forced}$ also scales as $1/R_\lambda$.

Second, we consider numerically simulated forced box turbulence or SFPBT, for which the energy injection is ensured at a given scale L_f, or a wavenumber $k_f \sim 1/L_f$. Then, energy $E(k_f)$ is continuously provided at the wavenumber k_f. Term $LS_{forced}(r)$ is proportional to the energy at that scale times velocity gradients at that scale, so it can be written as the energy at the scale r times the strain felt by that scale because of the energy injected at scale L_f. Since the characteristic strain felt at any wavenumer k is given by (Danaila & Antonia 2009)

$$\tau(k) \sim \left[\int_0^k k^2 E(k) dk\right]^{-1/2}, \tag{2.19}$$

the strain at the scale r becomes $s(k) \propto \left[E(k_f) * k_f^3\right]^{1/2}$, or, in real space

$$s(r) \propto \left[\frac{\overline{(\delta u)^2}(L_f)}{L_f^2}\right]^{1/2} = \frac{\overline{(\delta u)^2}^{1/2}(L_f)}{L_f}, \tag{2.20}$$

which is a constant in r, as it is directly given by the large-scale injection. The last step is to write $LS_{forcing} \sim \overline{(\delta u)^2} \cdot s(r)$ and it is straightforward to show that

$$\mathcal{D}_{forcing} = \frac{\lambda}{u'} \cdot s(r) \equiv \frac{\lambda}{u'} \cdot \frac{\overline{(\delta u)^2}^{1/2}(L_f)}{L_f}. \tag{2.21}$$

It is very reasonable to consider that the energy injected will be proportional to the typical fluctuation u', so $u' \sim \left[\overline{(\delta u)^2}(L_f)\right]^{1/2}$. Then,

$$\mathcal{D}_{forcing} = \frac{\lambda}{L_f} \propto \frac{1}{R_\lambda}. \tag{2.22}$$

Therefore, for forced box turbulence, the constant C is not zero, as suggested by some data at small and moderate Reynolds numbers in Fig. 5, but is likely to be much smaller than the values of C for either decaying turbulence, or when turbulence is forced over a range of scales. For example, the estimated ratio of the large scale forcing term to S for the SFPBT of Fukayama *et al.* (2000) is about 1.6% at $R_\lambda = 70$ (estimated from their Fig. 5), while it is several orders of magnitude smaller than S at $R_\lambda = 460$ for the SFPBT of Gotoh *et al.* (2002). In this case, one expects $S{+}2G/R_\lambda$ to be very nearly zero.

3. G/R_λ

The considerations of section 2 point to $S + 2G/R_\lambda$ approaching zero at sufficiently large R_λ although the approach will differ in each flow. This is summarized in Fig. 1. At any finite R_λ, grid turbulence is furthest from stationarity. One expects the SFPBT data to lie close to the x axis. Given the uncertainties (e.g. noise contamination and/or inadequate spatial resolution in hot-wire measurements) in estimating S and G, it is unlikely that for $R_\lambda \geqslant 300$, one will be able to distinguish unambiguously how $S{+}2G/R_\lambda$ departs from zero between different flows.

The term G, defined by (2.5), can be rewritten

$$G = \frac{\overline{u^{*2}}\,\overline{(\partial^2 u^*/\partial x^{*2})^2}}{\overline{(\partial u^*/\partial x^*)^2}^2} \tag{3.1}$$

where the asterisk denotes normalization by the Kolmogorov scales. If local isotropy holds, so that $\overline{\epsilon} = \overline{\epsilon}_{iso} = 15\nu\overline{(\partial u/\partial x)^2}$, (3.1) can be rewritten as

$$\frac{2G}{R_\lambda} = 2 \times 15^{3/2} \int_0^\infty {k_1^*}^4 \phi_u^*(k_1^*) dk_1^*, \tag{3.2}$$

where $\phi_u^*(k_1^*)$ is the one-dimensional spectral density of u, defined such that $\int_0^\infty \phi_u(k_1) dk_1 =$

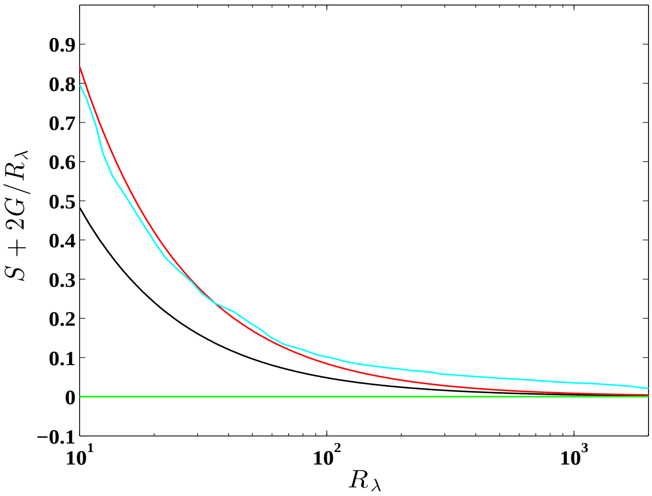

FIGURE 1. Dependence of $S+2G/R_\lambda$ (Eq. (2.6)) on R_λ in different flows. (a) grid turbulence (red), R=0.9, and n=1.1; (b) along the axis of a round jet (black), R=2/3; (c) ideal stationary state (green); (d) Eddy-Damped Quasi-Normal Markovian (EDQNM) simulation of decaying homogeneous isotropic turbulence (HIT) (light blue) (Meldi & Sagaut 2013).

$\overline{u^2}$. If there is a departure from local isotropy, then $2G/R_\lambda$ is estimated using

$$\frac{2G}{R_\lambda} = 2\nu \frac{\int_0^\infty {k_1}^4 \phi_u(k_1) dk_1}{[\int_0^\infty {k_1}^2 \phi_u(k_1) dk_1]^{3/2}}. \tag{3.3}$$

Departure from local isotropy occurs when the large scale anisotropy is felt in the inertial range. However, when this occurs, it does not affect the results discussed in this paper. Indeed, the inertial range does not extend beyond $k^* \simeq 0.05$ irrespective of the R_λ (*e.g.* Ishihara *et al.* (2009), Yoffe (2012)). As it will be seen later (see for example Fig. 7), the contribution to $\int_0^\infty {k_1^*}^4 \phi_u^*(k_1^*) dk_1^*$ from the wavenumber range $0 \leqslant k^* < 0.05$, which include the inertial range, is negligible in comparison to the contribution from the spectra region above $k^* = 0.05$. Thus, any large-scale anisotropy within the inertial range cannot affect the calculation of G/R_λ.

There is ample evidence in the literature to indicate that the integrals in (3.2) or (3.3) will rapidly converge to constant values with increasing R_λ. This behaviour follows from the collapse of the dissipative part of $\phi_u(k_1)$ when it is normalized with u_K and η, e.g. Saddoughi & Veeravalli (1994). This collapse does not require R_λ to be large (Antonia *et al.* 2014), nor does it require local isotropy (LI) to be satisfied rigorously; it does however break down when R_λ is small enough, typically smaller than 40. A value as small as 20 was identified by Djenidi *et al.* (2014).

4. Results for S in a wide range of turbulent flows

Estimates of $2G/R_\lambda$ for the flows considered in Fig. 1 are shown in Fig. 2. Also included are estimates inferred from measured spectra along the axis of a pipe by Rosenberg *et al.* (2013) (the maximum value of R_λ for their measurements was 1362) also on the axis of a plane far-wake (Champagne 1978). Since hot-wire measurements have good temporal and spatial resolution for $R_\lambda \leqslant 30$, the measured spectra were used to estimate $2G/R_\lambda$ directly in this range of Reynolds numbers. For $R_\lambda > 30$, a uniform treatment was applied to the measured distributions of $\phi_u^*(k_1^*)$ primarily to avoid the effects of noise contamination and possible inadequate spatial resolution. The portion of the measured spectra beyond $k_1^*{\approx}0.3$ was ignored and the distributions were extrapolated using a reference spectrum. There is now cogent analytical arguments describe by Antonia *et al.* (2014), supported by strong experimental and numerical evidence at low Reynolds numbers, for extrapolating the dissipative range of the spectrum. Antonia *et al.* (2014) showed that the collapse of the Kolmogorov-normalized spectrum in the dissipative range does on hinge on local isotropy. Nor does it require the Reynolds number to be large. It is important to stress that the collapse is supported by experimental and numerical data at low Reynolds numbers (for which spatial resolution is not an issue), hence justifying the extrapolation as R_λ increases. The extrapolation avoids both the spatial resolution and high frequency (measurement) noise issues as R_λ increases. Further, the arguments underpinning the extrapolation become all the more justifiable since there is a decreasing likelihood that the inhomogeneities in the large scales will affect the small scales when R_λ increases. Thus, any sufficiently well resolved numerical or experimental spectrum can be used for extrapolating the measured spectra whose dissipative range is not fully resolved. Here we used the model spectrum of Pope (2000) mainly for convenience. The constants were calibrated against well resolved DNS spectra (Abe *et al.* 2009*a*) on the centreline of a channel flow, where the departure from LI is small and remained unchanged for all the flows used in Fig. 2 (details of the procedure can be found in Tang *et al.* (2015b); see also Lee *et al.* (2013)). It is important to stress that the model is mainly used as a curve fit to the DNS data in the region $k* \geqslant 0.3$ to carry out the extrapolation of the measured spectra. Further, the use of $k^{*-5/3}$ in the model has not biased the values of G/R_λ that have been estimated from the extrapolated spectra, since, as commented earlier, the contribution from this part of the spectrum is insignificant. As an example, one set of extrapolated spectra for active grid turbulence (Larssen & Devenport 2011) with R_λ in the range 100-1360 are shown in Fig 3. For $R_\lambda > 30$, $2G/R_\lambda$ was estimated using the extrapolated spectra. The larger values of $2G/R_\lambda$ at small R_λ in Fig. 2 reflects, to a large extent, the systematic departure of Kolmogorov normalized spectra of u, in particular the systematic increase of the spectral density in the dissipation range (e.g. Mansour & Wray 1994; Djenidi *et al.* 2014).

For grid turbulence, and along the axis of a round jet, $2G/R_\lambda$ is constant ($\approx$0.53$\pm$0.1) for R_λ>70. For SFPBT, the constancy of $2G/R_\lambda$ (≈ 0.53) is achieved at small R_λ; however, it would now seem that, for this type of forced turbulence, $2G/R_\lambda$ starts to increase slowly with R_λ, when the latter exceeds a value of about 300 (e.g. Ishihara *et al.* 2007; Gauding 2014). The light blue curve, inferred from the EDQNM simulation (Meldi & Sagaut 2013), approaches the same constant value ($\approx$0.53) as the other experimental data in Fig. 2 only for $R_\lambda \approx 10^3$. This slow approach, which can also be seen in Fig. 1, is different from that exhibited by all the other data and may reflect differences in the initial conditions between simulation and experiments.

In what follows, we consider data for $-S$ obtained by various authors in a wide range of flows. Separate plots are used (Figs. 4, 5, 6), with the same x and y scales. The theoretical distribution of Qian (1994) is shown, as reference, on each plot. The value of 0.53 inferred from Fig. 2 is also shown in each plot. With the exception of the channel and pipe flows, the flows in Fig. 4 are of the decaying type. The red and black curves are estimated from $S + 2G/R_\lambda = C/R_\lambda$ by assuming that $2G/R_\lambda$=constant (≈ 0.53, when R_λ>70). For the red curve (grid turbulence), C, estimated from Eq. (2.7), is equal to 8.8 (n was 1.2 as in the experiment of Lee *et al.* (2013) and $R = 0.9$). For the black curve (axis of axisymmetric jet), C, estimated from Eq. (2.10), is equal to 4.8 ($R = 2/3$, (Thiesset *et al.* 2014)). Although there are relatively few data available in the literature

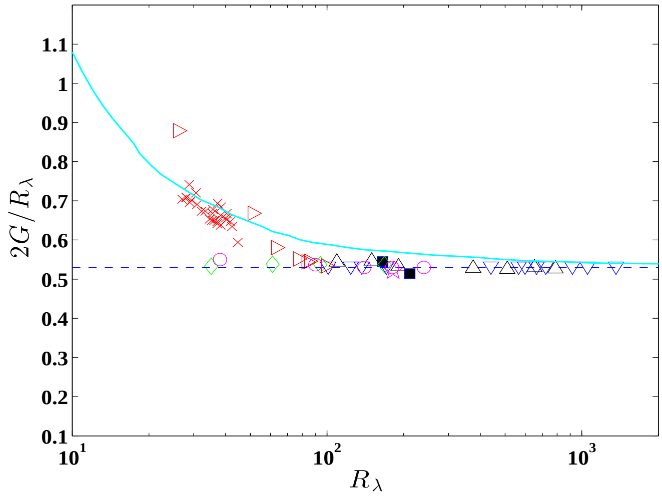

FIGURE 2. Dependence of $2G/R_\lambda$ on R_λ in different flows. (a) grid turbulence: ▷, unpublished passive grid data of Zhou & Antonia (2000); ▽, Larssen & Devenport (2011), active grid; ×, Lee *et al.* (2013), passive grid; (b) axis of pipe: △, Rosenberg *et al.* (2013); (c) axis of plane far-wake, ☆, Champagne (1978); (c) SFPBT: ◇, Jimenez *et al.* (1993); ◯, Yeung & Zhou (1997); (d) jet axis: ■, Lefeuvre *et al.* (2015); (e) light blue curve: EDQNM (Meldi & Sagaut 2013) for HIT. The horizontal line indicates the value of 0.53.

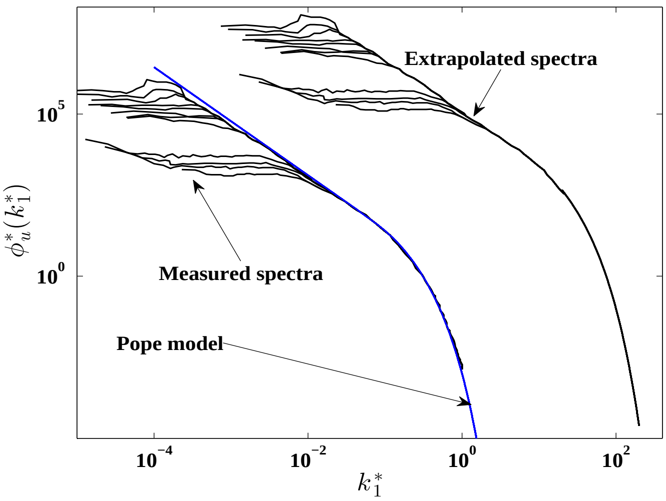

FIGURE 3. Measured and extrapolated spectra for the active grid turbulence, data of Larssen & Devenport (2011) with R_λ in the range 100-1360. The extrapolated spectra are offset by two orders of magnitude along both x and y axes.

in the range $10^2 < R_\lambda < 10^3$, the trend with R_λ of these data provides reasonable support for the curves. The smallest values of -S correspond to the centreline of the channel and the axis of the pipe (Antonia & Pearson 2000). There seems little doubt that for $R_\lambda \leqslant 200$, where the FRN effect must be important, $-S$ can vary significantly from flow to flow. This variation is reflected in the variation of C, which in essence represents the different physical processes at large scales that contribute to the one-point energy

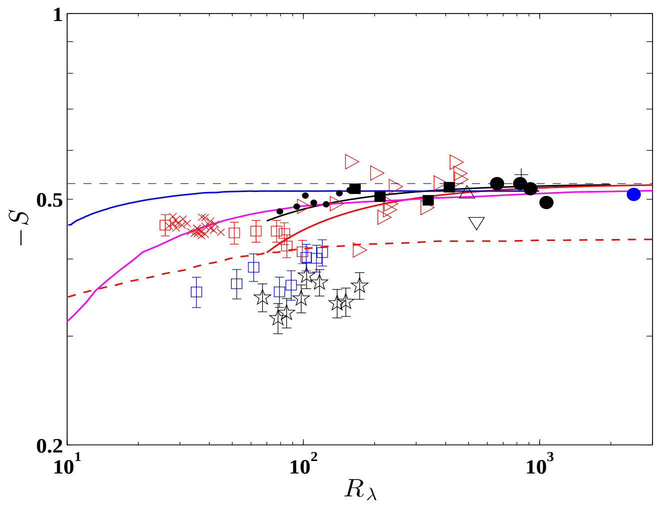

FIGURE 4. Dependence of measured values of -S on R_λ in different flows and from two separate EDQNM simulation for decaying HIT. (a) centreline of a fully developed channel flow (❒) and pipe (☆), Antonia & Pearson (2000). (b) along the axis of a round jet: •, Mi *et al.* (2013); ▽, Friehe *et al.* (1971); +, Kahalerras *et al.* (1998); △, (Burattini, private communication); ■, Lefeuvre *et al.* (2015). (c) grid turbulence: ×, Lee *et al.* (2013); ▷, Mydlarski & Warhaft (1996); ❒, unpublished data of Zhou & Antonia (2000). (d) along the axis of a plane jet, ●, Zhou *et al.* (2005); along the axis of the ONERA wind tunnel, ●, measurements of Kahalerras *et al.* (1998); see Bos *et al.* (2012); blue curve, Qian (1994); pink and red dashed curves correspond to EDQNM of Meldi & Sagaut (2013) and Bos *et al.* (2012) respectively. Red and black curves, inferred from Eq. (2.6) by assuming $2G/R_\lambda$=constant (≈ 0.53 for R_λ>70), correspond to grid turbulence, and the axis of a round jet, respectively. The horizontal line indicates the value of 0.53.

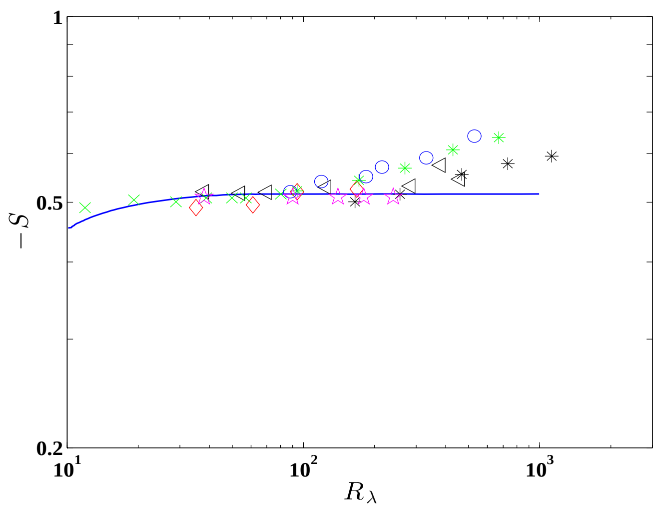

FIGURE 5. Dependence of -S on R_λ for SFPBT. ◇, Jimenez *et al.* (1993); ×, Kerr (1985); ◁, Gotoh *et al.* (2002); ☆, Yeung & Zhou (1997); ○, Gauding (2014) (k^*_{max}=2.53∼4.99); ∗ (k^*_{max}=1) and ∗ (k^*_{max}=2) correspond to Ishihara *et al.* (2007); blue curve, Qian (1994).

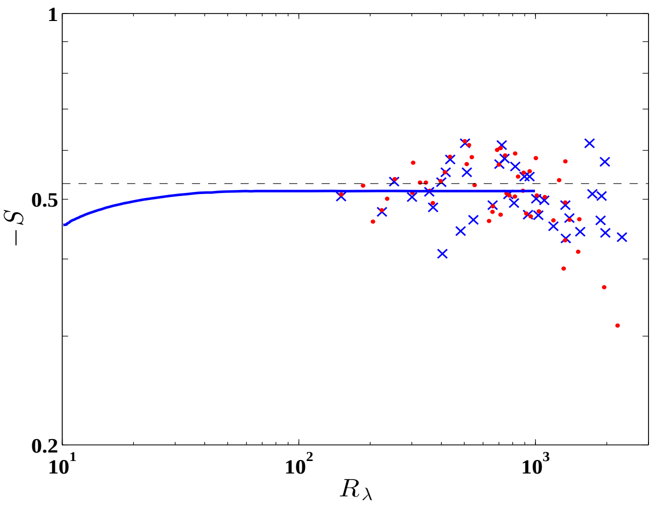

FIGURE 6. Dependence of -S on R_λ in flow between counter-rotating disks. •, Tabeling *et al.* (1996); ×, Belin *et al.* (1997); blue curve, Qian (1994); the horizontal line indicates the value of 0.53.

budget in different flows. For example, one expects the large scale contribution to the one-point energy budget in the channel and pipe by turbulent diffusion (Tang *et al.* 2015b). It is also evident that for a given flow, $-S$ may depend on the initial conditions (e.g. Lavoie *et al.* 2007; Lee *et al.* 2013); we also note that, for the HIT simulations of Antonia & Orlandi (2004); Burattini *et al.* (2008), $-S$ is 0.5 for $50 < R_\lambda < 60$ whereas most of the measured values are somewhat smaller at such Reynolds numbers. Despite the scatter, the data for -S on the jet axis (Mi *et al.* 2013; Friehe *et al.* 1971; Kahalerras *et al.* 1998) are in satisfactory agreement with the black curve. The major difficulty here is the high turbulence intensity level on the jet axis and its effect on Taylor's hypothesis (TH). We suspect that the large values of -S (=0.68 and 0.80) reported by Champagne *et al.* (1977) (they are not included in Fig. (4)) were adversely affected by the corrections that were applied to TH. The two EDQNM distributions in Fig. 4 approach different values at large R_λ, possibly reflecting differences in the initial conditions. We recall once again that self-preserving HIT ($n = 1$) at all scales is possible only when R_λ is constant, regardless of its value (see Meldi & Sagaut (2013); Djenidi & Antonia (2015)). In this case, S can only be constant, in conformity with $K41$ (see the discussion in section 2).

Only SFPBT data are shown in Fig. 5; -S is virtually constant for $R_\lambda > 20 - 40$. This is in quite good accord with the analytical prediction (-S=0.515 for $R_\lambda > 40$) of Qian (1994, 2003). DNS data of Gotoh *et al.* (2002) indicated that for $38 \leqslant R_\lambda \leqslant 284$, -$S$ is approximately constant ($\simeq 0.53$). For R_λ=381 and 460, $-S$ was 0.574 and 0.545 respectively, suggesting a possible small increase in $-S$ with increasing R_λ. This has since been confirmed by the DNS data of Ishihara *et al.* (2007) which suggest an increase of -S according to (1.2) with α= 0.11. Since this turbulence should be stationary, the increase reflects an increase of $2G/R_\lambda$ with R_λ; this issue will be discussed later in the context of Fig. 7.

Various statistics for $\partial u/\partial x$ were presented by Tabeling *et al.* (1996) and Belin *et al.* (1997) for a flow of helium gas at low temperature between two counter-rotating disks over an impressively large range of R_λ: 150 to 5040 (Tabeling *et al.* 1996) and 150 to 2300 (Belin *et al.* 1997). In the context of this paper, these results are useful for two reasons.

Firstly, S has been collected in the same flow. Secondly, since the flow is of the forced type, the range of R_λ should be large enough to allow an exploration of α beyond the range of R_λ that is associated with FRN effects. Moisy *et al.* (1999) showed that for this flow, $\overline{(\delta u^*)^3}/r^*$ displays a reasonable plateau, with a magnitude of about 0.77, which is quite close to Kolmogorov's 4/5 law, when R_λ exceeds 1000. Antonia & Burattini (2006) showed that for this type of flow, $R_\lambda \simeq 1000$ should be sufficient for FRN effects to cease being important. The data of Tabeling *et al.* (1996) were not included in Sreenivasan & Antonia's compilations (Sreenivasan & Antonia 1997) for S and F, the flatness factor of $\partial u/\partial x$, mainly because of a (slow) drop off in S & F beyond $R_\lambda \simeq 700-800$, which was reported to coincide with a transition to a new state of turbulence. This behaviour was reproduced in the later experiment by Belin *et al.* (1997) and the values of S and F seemed unaffected at least up to $R_\lambda \simeq 1000$. Both sets of data for S are shown in Fig. 6, up to $R_\lambda \simeq 2000$. The transitional behaviour is difficult to discern in $-S$ but can be more easily seen in F and higher order moments of $\partial u/\partial x$ (which are not shown here). It is clear however, that, allowing for the scatter, the Belin *et al.* (1997) data suggest, as the authors indicate, that $-S$ remains constant ($\simeq 0.50$) over the whole range of R_λ, up to $R_\lambda \simeq 2000$. This is consistent with our expected behaviour (section 2) of $-S$ when forcing is applied.

The high wavenumber part of $k^{*4}E^*(k^*)$ (see blue curves in Fig. 7), where $E(k)$ is the 3D energy spectrum, increases systematically with R_λ implying nonconformity with Kolmogorov scaling. This contrasts with the arguments put forward in Antonia *et al.* (2014), the behaviour of spectra from lower R_λ DNSs of SFPBT as well as that for experimental data in a wide range of flows at comparable if not larger R_λ than for Ishihara *et al.* (2007). Figure 7 also shows the distributions of $k^{*4}E^*(k^*)$ of Gotoh *et al.* (2002) (R_λ=38 $\sim$ 460), Jimenez *et al.* (1993) (R_λ=35 $\sim$ 168) and Yeung & Zhou (1997) (R_λ=38 $\sim$ 240) for SFPBT. Whilst the spectra of Gotoh *et al.* (2002), Jimenez *et al.* (1993), and Yeung & Zhou (1997) collapse at high wavenumbers over the range $38 \leqslant R_\lambda \leqslant 460$, those of Ishihara *et al.* (2007) exhibit a systematic increase with R_λ (a similar trend has been observed by Gauding (2014), private communication); this is consistent with the increase of $-S$ with R_λ in Fig. 5. It is not clear why the spectra of Ishihara *et al.* (2007) do not conform with Kolmogorov scaling, in particular with the 1st similarity law. Nevertheless, Ishihara *et al.* (2005, 2007, 2009) leave open the possibility, based on fitting to $k^{*4}E^*(k^*)$ for $k^* > 0.5$, that as $R_\lambda \to \infty$, $-S$ "approaches a constant independent of R_λ but the approach may be slow".

Contrary to Fig. 7, the distributions of $k_1^{*4}\phi_1^*(k_1^*)$ in Fig. 8, where the maximum R_λ is larger than in Fig. 7, do not exhibit any obvious dependence on R_λ. Notwithstanding the scatter and the peeling off at decreasing values of k_1^* with increasing R_λ of some of the data, the distributions cluster together in accord with Kolmogorov scaling and the constancy of G/R_λ in Fig. 2.

We conclude this section by examining the dependence on R_λ of $S_{\delta u}$, the skewness of δu, viz. $S_{\delta u} = \overline{(\delta u)^3}/\overline{(\delta u)^2}^{3/2}$, for most of the flows used in Fig. 4. Figure 9 highlights the relatively strong variation with R_λ of both the shape and magnitude of $S_{\delta u}$ at least up to $R_\lambda \simeq 1000$. Whilst the variation with R_λ is systematic for a given flow, e.g. the centreline of the channel (solid red curves) or grid turbulence (broken blue curves), the magnitude of $S_{\delta u}$ is larger for grid turbulence than the channel flow despite R_λ being smaller in grid turbulence. This behaviour is of course consistent with Fig. 4. For all the data in Fig. 9, the resolution of the single hot wire, as measured by the ratio l_w/η (l_w is the length of the wire) is adequate since l_w/η remains in the range 0.5-3. For $R_\lambda \geqslant 500$ (the plane & circular jet data as well as the Modane data at R_λ=2500), the distributions

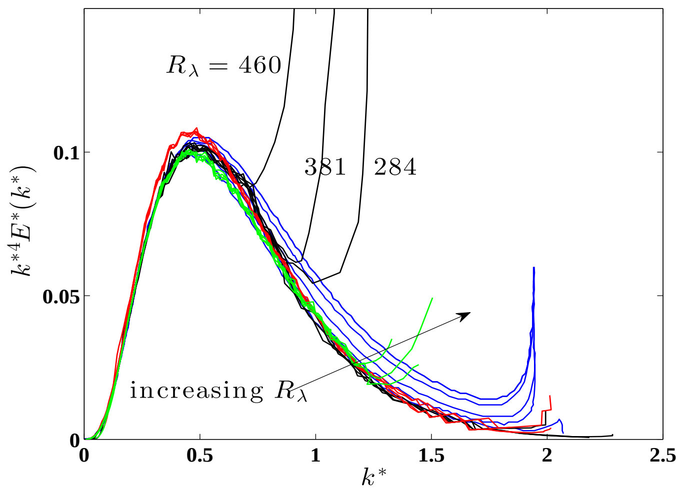

FIGURE 7. Normalized three-dimensional DNS spectra $k^{*4}E^*(k^*)$ for SFPBT. Blue curves, (Ishihara *et al.* 2007), R_λ=94, 173, 268, 429, and 675 respectively; the arrow indicates the direction R_λ increases. Black curves, (Gotoh *et al.* 2002), R_λ=38, 54, 70, 125, 284, 381, and 460 respectively. Red curves, (Jimenez *et al.* 1993), R_λ=35, 61, 94, and 168 respectively. Green curves, (Yeung & Zhou 1997), R_λ=38, 90, 140, 180, and 240 respectively.

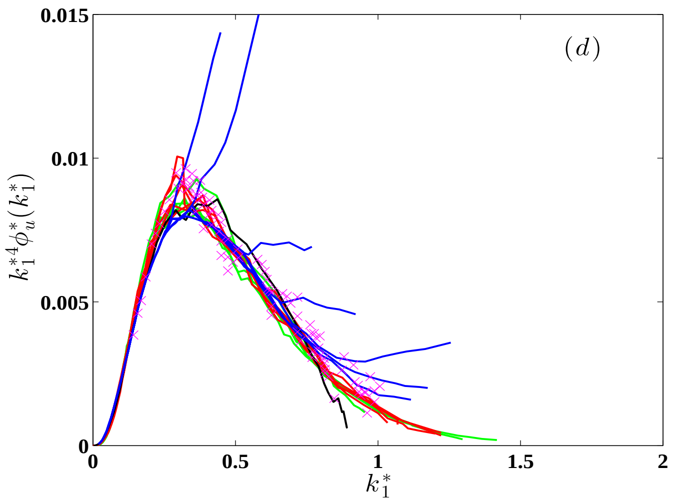

FIGURE 8. Normalized one-dimensional spectra $k_1^{*4}\phi_1^*(k_1^*)$. Red curves, Antonia *et al.* (2014), R_λ=41-140; blue curves, Rosenberg *et al.* (2013), R_λ=109-788; ×, Larssen & Devenport (2011), R_λ=100-1360; black curve, DNS data of Gotoh *et al.* (2002), R_λ=460; green curves, DNS data on the centreline of a channel flow (Abe *et al.* 2009*b*), R_λ=34-66.

of $S_{\delta u}$ seem to collapse reasonably well at small r^*, up to $r^* \simeq 200$. The rate at which $S_{\delta u}$ decreases as r^* increases slows down for $r^* \geqslant 20$ but there is no clear indication that $S_{\delta u}$ becomes constant, even for R_λ=25000. K41 requires the constant value, $(-S_{\delta u})_{IR}$ say, to be equal to $4/5C_K^{-3/2}$ where C_K is the Kolmogorov constant, i.e. $\overline{(\delta u)^2} = C_K(\overline{\varepsilon} r)^{2/3}$. The EDQNM result of Bos *et al.* (2012) appears to approach a plateau in the inertial range; their data suggest that $C_K \simeq 2.2$ so that $(-S_{\delta u})_{IR} = 0.25$. Despite the very large R_λ, the

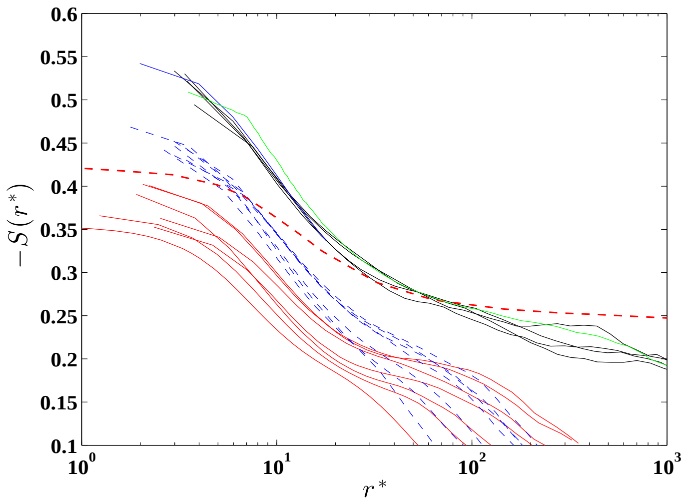

FIGURE 9. Skewness structure functions in different flows. (a) Red curves, centreline of a fully developed channel flow, Antonia & Pearson (2000), R_λ=33-120 (l_w/η=0.5-3.0). (b) Blue dashed curves, grid turbulence, Zhou & Antonia (2000), R_λ=26-99, (l_w/η=0.6-2.5). (c) Black curves, plane jet axis, Zhou *et al.* (2005), R_λ=660-1067 (l_w/η=1.4-2.3). (d) Blue solid curve, axis of a round jet, Kahalerras *et al.* (1998), R_λ=835 ($l_w/\eta = 2.5$). (e) Green curve, axis of the ONERA wind tunnel, measurements of Kahalerras *et al.* (1998); see Bos *et al.* (2012) R_λ=2500 ($l_w/\eta = 1.14$). Red dashed curve, EDQNM, Bos *et al.* (2012), R_λ=25000. Note that for all experimental data, $l_w/\eta \leqslant 3.0$.

plateau for $\overline{(\delta u)^2}/(\bar{\epsilon} r)^{2/3}$ (the dashed red curve) is not yet reached (Fig. 3 of Bos *et al.* (2012)), reinforcing Antonia & Burattini's (2006) finding that, for decaying HIT, R_λ should probably exceed 10^6 before the inertial range is established unequivocally.

5. Concluding discussion

Overall, Fig. 4 strongly supports the idea that in each flow -S approaches the same constant value as R_λ increases but this approach differs from flow to flow. This vindicates the suggestion by Thiesset *et al.* (2014) that previous attempts at testing the R_λ dependence of properties of the SSM, which indiscriminately lumped together data from all types of laboratory flows, are either not meaningful or, at the very least, should be treated with caution. Further, even when the exponent is estimated from the same flow, one needs to be sure that R_λ is sufficiently large for the FRN effect to have disappeared. This is unlikely to be an easy task in decaying-type flows in view of the results in Antonia & Burattini (2006).

Since the flow dependent constant C is positive (although varying from flow to flow and possibly from position to position in a given flow), -S should remain smaller than its asymptotic constant (≈ 0.53) until C/R_λ becomes negligible. As predicated by Qian (1994), -S cannot grow unboundedly as R_λ increases. This is contrary to the predictions from lognormal and fractal models, (e.g. Van Atta & Antonia 1980; Frisch *et al.* 1978), but is consistent with the vortex tube model of Tennekes (1968) and the heuristic model of Saffman (1970).

Interestingly, the constancy of S which is equal to $S_{\delta u}$ in the limit $r^* \to 0$, reflects complete self-preservation, or self-preservation at all scales of motion when R_λ is very high. In this case, $S_{\delta u}$ should collapse onto a single curve, regardless of R_λ and exhibit

3 plateaux, one at small r^* ($S_{\delta u} = S$=const), one in the IR ($S_{\delta u} = (S_{\delta u})_{IR}$=const), and one ($S_{\delta u}$=0) at large r^* ($> L^*$). The constraint imposed by $K41$, viz. S=const, and $(S_{\delta u})_{IR}$=const, is therefore subsumed within this more general framework. Although Figs. 4, 6 and 9 support the constancy of S for laboratory flows, Fig. 9 is a reminder that the constancy of $(S_{\delta u})_{IR}$ may be out of reach in the laboratory, at least for decaying turbulence. One expects the constancy of S and $(S_{\delta u})_{IR}$ to be obtained in forced HIT but, as illustrated in Figs. 5 and 7, this has yet to be confirmed by DNSs for forced periodic box turbulence.

The constancy of -S at sufficiently large R_λ implied by Figs. 4 and 6, which contrasts with (1.2), should not be too surprising given that the constraint of equation (2.6) is based on the Navier-Stokes (N-S) equations. It is worth recalling, in the context of the phenomenological model of Kolmogorov (1962), that, over the inertial range, $\overline{(\delta u)^3}$ is constrained to vary proportionately to r, provided R_λ is sufficiently large. All small scale intermittency models have had to satisfy this constraint. Future research may be able to verify that normalised higher order moments of $\partial u/\partial x$, e.g. the flatness factor ($F = \overline{(\partial u/\partial x)^4}/\overline{(\partial u/\partial x)^2}^2$) of $\partial u/\partial x$, may like -S, be also bounded at sufficiently large R_λ, once the appropriate constraint derived from the N-S equations is understood. Such a possibility was considered by Qian (1986).

The financial support of the Australian Research Council (ARC) is acknowledged.

REFERENCES

Abe, H., Antonia, R. A. & Kawamura, H. 2009*a* Correlation between small-scale velocity and scalar fluctuations in a turbulent channel flow. *J. Fluid Mech.* **627**, 1–32.

Abe, H., Antonia, R. A. & Kawamura, H. 2009*b* Correlation between small-scale velocity and scalar fluctuations in a turbulent channel flow. *J. Fluid Mech.* **627**, 1–32.

Antonia, R. A. & Burattini, P. 2006 Approach to the 4/5 law in homogeneous isotropic turbulence. *J. Fluid Mech.* **550**, 175–184.

Antonia, R. A., Djenidi, L. & Danaila, L. 2014 Collapse of the turbulent dissipation range on Kolmogorov scales. *Phys. Fluids* **26**, 045105.

Antonia, R. A. & Orlandi, P. 2004 Similarity of decaying isotropic turbulence with a passive scalar. *J. Fluid Mech.* **505**, 123–151.

Antonia, R. A. & Pearson, B. R. 2000 Reynolds number dependence of velocity structure functions in a turbulent pipe flow. *Flow, Turb. and Comb.* **64**, 95–117.

Antonia, R. A., Zhou, T., Danaila, L. & Anselmet, F. 2000 Streamwise inhomogeneity of decaying grid turbulence. *Phys. Fluids* **12**, 3086.

Batchelor, G.K. 1953 *The theory of homogeneous turbulence*. CUP.

Batchelor, G. K. & Townsend, A. A. 1947 Decay of vorticity in isotropic turbulence. *Proc. R. Soc. London, Ser. A* **190**, 534–550.

Belin, F., Maurer, J., Tabeling, P. & Willaime, H. 1997 Velocity gradient distributions in fully developed turbulence: experimental study. *Phys. Fluids* **9**, 3843–3850.

Bos, W. J. T., Chevillard, L., Scott, J. F. & Rubinstein, R. 2012 Reynolds number effect on the velocity increment skewness in isotropic turbulence. *Phys. Fluids* **24**, 015108.

Burattini, P., Antonia, R. A. & Danaila, L. 2005 Similarity in the far field of a turbulent round jet. *Phys. Fluids* **17**, 025101.

Burattini, P., Lavoie, P. & Antonia, R. A. 2008 Velocity derivative skewness in isotropic turbulence and its measurement with hot wires. *Exp. Fluids* **45**, 523–535.

Champagne, F. H. 1978 The fine-scale structure of the turbulent velocity field. *J. Fluid Mech.* **86**, 67–108.

Champagne, F. H., Friehe, C. A., LaRue, J. C. & Wyngaard, J. C. 1977 Flux measurements, flux estimation techniques, and fine scale turbulence measurements in the unstable surface layer over land. *J. Atmos. Sci.* **34**, 515–530.

Danaila, L., Anselmet, F., Zhou, T. & Antonia, R. A. 1999 A generalization of Yaglom's equation which accounts for the large-scale forcing in heated decaying turbulence. *J. Fluid Mech.* **391**, 359–372.

Danaila, L. & Antonia, R. A. 2009 Spectrum of a passive scalar in moderate Reynolds number homogeneous isotropic turbulence. *Phys. Fluids* **21**, 111702.

Djenidi, L. & Antonia, R. A. 2015 A general self-preservation analysis for decaying homogeneous isotropic turbulence. *J. Fluid Mech.* **773**, 345–365.

Djenidi, L., Tardu, S.F., Antonia, R.A. & Danaila, L. 2014 Breakdown of Kolmogorov's first similarity hypothesis in grid turbulence. *J. Turb.* **15**, 596–610.

Friehe, C.A., Atta, C.W. Van & Gibson, C.H. 1971 Jet turbulence: Dissipation rate measurements and correlations. *AGARD Turbulent Shear Flows* **18**, 1–7.

Frisch, U. 1995 *Turbulence: The Legacy of A. N. Kolmogorov.* CUP.

Frisch, U., Sulem, P. L. & Nelkin, M. 1978 A simple dynamical model of intermittent fully developed turbulence. *J. Fluid Mech.* **87**, 719–736.

Fukayama, D., Oyamada, T., Nakano, T., Gotoh, T. & Yamamoto, K. 2000 Longitudinal structure functions in decaying and forced turbulence. *J. Phys. Soc. Jpn.* **69**, 701–715.

Gauding, M. 2014 *Statistics and Scaling Laws of Turbulent Scalar Mixing at High Reynolds Numbers.* PhD Thesis, RWTH Aachen University.

George, W. K. 1992 The Decay of Homogeneous Isotropic Turbulence. *Phys. Fluids* **5**, 1–29.

George, W. K., Wang, H., Wollblad, C. & Johansson, T. G. 2001 'Homogeneous Turbulence' and Its Relation to Realizable Flows. *14th Australasian Fluid Mechanics Conference* **Adelaide University, Adelaide, Australia 10-14 December**.

Gibson, C. H., Stegen, G. R. & Williams, R. B. 1970 Statistics of the fine structure of turbulent velocity and temperature fields at high Reynolds number. *J. Fluid Mech.* **41**, 153–167.

Gotoh, T., Fukayama, D. & Nakano, T. 2002 Velocity field statistics in homogeneous steady turbulence obtained using a high-resolution direct numerical simulation. *Phys. Fluids* **14**, 1065–1081.

Ishihara, T., Gotoh, T. & Kaneda, Y. 2009 Study of high-Reynolds number isotropic turbulence by direct numerical simulation. *Annu. Rev. Fluid Mech.* **41**, 165–80.

Ishihara, T., Kaneda, Y., Yokokawa, M., Itakura, K. & Uno, A. 2005 Energy Spectrum in the Near Dissipation Range of High Resolution Direct Numerical Simulation of Turbulence. *J. Phys. Soc. Japan* **72**, 983–986.

Ishihara, T., Kaneda, Y., Yokokawa, M., Itakura, K. & Uno, A. 2007 Small-scale statistics in high-resolution direct numerical simulation of turbulence: Reynolds number dependence of one-point velocity gradient statistics. *J. Fluid Mech.* **592**, 335–366.

Jimenez, J., Wray, A. A., Saffman, P. G. & Rogallo, R. S. 1993 The structure of intense vorticity in isotropic turbulence. *J. Fluid Mech.* **255**, 65–90.

Kahalerras, H., Malecot, Y. & Gagne, Y. 1998 Intermittency and Reynolds number. *Phys. Fluids* **10**, 910–921.

Karman, T. & Howarth, L. 1938 On the statistical theory of isotropic turbulence. *Proc. Roy. Soc. Lond. Ser. A Math. Phys. Sci.* **164**, 192–215.

Kerr, R. M. 1985 Higher-order derivative correlations and the alignment of small-scale structures in isotropic numerical turbulence. *J. Fluid Mech.* **153**, 31–58.

Kolmogorov, A . N . 1941a Local structure of turbulence in an incompressible fluid for very large Reynolds numbers. *Dokl. Akad. Nauk SSSR* **30**, 299–303.

Kolmogorov, A . N . 1941b Dissipation of energy in the locally isotropic turbulence. *Dokl. Akad. Nauk SSSR* **32**, 19–21.

Kolmogorov, A . N . 1962 A refinement of previous hypotheses concerning the local structure of turbulence in a viscous incompressible fluid at high Reynolds number. *J. Fluid Mech.* **13**, 82–85.

Larssen, J. V. & Devenport, W. J. 2011 On the generation of large-scale homogeneous turbulence. *Exp. Fluids* **50**, 1207–1223.

Lavoie, P., Djenidi, L. & Antonia, R. A. 2007 Effects of initial conditions in decaying turbulence generated by passive grids. *J. Fluid Mech.* **585**, 395–420.

Lee, S. K., Djenidi, L., Antonia, R. A. & Danaila, L. 2013 On the destruction coefficients for slightly heated decaying grid turbulence. *International Journal of Heat and Fluid Flow* **43**, 129–136.

Lefeuvre, N., Djenidi, L. & Antonia, R. A. 2015 Decay of mean energy dissipation rate on the axis of a turbulent round jet. *The 9th Symposium on Turbulence and Shear Flow Phenomena (TSFP-9)* pp. (June 30th–July 3rd, Melbourne, Australia).

Lindborg, E. 1999 Correction to the four-fifths law due to variations of the dissipation. *Phys. Fluids* **11**, 510.

Mansour, N. N. & Wray, A. A. 1994 Decay of isotropic turbulence at low Reynolds number. *Phys. Fluids* **6**, 808–813.

Meldi, M. & Sagaut, P. 2013 Further insights into self-similarity and self-preservation in freely decaying isotropic turbulence. *J. Turb.* **14**, 24–53.

Mi, J., Xu, M. & Zhou, T. 2013 Reynolds number influence on statistical behaviors of turbulence in a circular free jet. *Phys. Fluids* **25**, 075101.

Moisy, F., Tabeling, P. & Willaime, H. 1999 Kolmogorov Equation in a Fully Developed Turbulence Experiment. *Phys. Rev. L.* **82**, 3994–3997.

Mydlarski, L. & Warhaft, Z. 1996 On the onset of high- Reynolds-number grid-generated wind tunnel turbulence. *J. Fluid Mech.* **320**, 331–368.

Pope, S. B. 2000 Turbulent flows. Cambridge University Press.

Qian, J. 1986 A closure theory of intermittency of turbulence. *Phys. Fluids* **29**, 2165.

Qian, J. 1994 Skewness factor of turbulent velocity derivative. *Acta Mechanica Sinica* **10**, 12–15.

Qian, J. 1999 Slow decay of the finite Reynolds number effect of turbulence. *Phys. Rev. E* **60**, 3409.

Qian, J. 2003 An equality about the velocity derivative skewness in turbulence. *Phys. Fluids* **15**, 1005.

Rosenberg, B. J., Hultmark, M., Vallikivi, M., Bailey, S. C. C. & Smits, A. J. 2013 Turbulence spectra in smooth- and rough-wall pipe flow at extreme Reynolds numbers. *J. Fluid Mech.* **731**, 46–63.

Saddoughi, S. G. & Veeravalli, S . V . 1994 Local isotropy of turbulent boundary layers at high Reynolds number. *J. Fluid Mech.* **268**, 333–372.

Saffman, P. G. 1970 Dependence on Reynolds number of high-order moments of velocity derivatives in isotropic turbulence. *Phys. Fluids* **13**, 2193–2194.

Speziale, C. G. & Bernard, P. S. 1992 The energy decay in self-preserving isotropic turbulence revisited. *J. Fluid Mech.* **241**, 645–667.

Sreenivasan, K. & Antonia, R. A. 1997 The phenomenology of small-scale turbulence. *Annu. Rev. Fluid Mech.* **29**, 435–472.

Tabeling, P., Zocchi, G., Belin, F., Maurer, J. & Willaime, H. 1996 Probability density functions, skewness, and flatness in large Reynolds number turbulence. *Phys. Rev. E* **53**, 1613–1621.

Tang, S. L., Antonia, R. A., Djenidi, L., Abe, H., Zhou, T., Danaila, L. & Zhou, Y. 2015b Transport equation for the mean turbulent energy dissipation rate on the centreline of a fully developed channel flow. *J. Fluid Mech.* **777**, 151–177.

Tang, S. L., Antonia, R. A., Djenidi, L. & Zhou, Y. 2015a Consequence of self-preservation in a turbulent far-wake. *The 9th Symposium on Turbulence and Shear Flow Phenomena (TSFP-9)* pp. (June 30th–July 3rd, Melbourne, Australia).

Tennekes, H. 1968 Simple model for the small-scale structure of turbulence. *Phys. Fluids* **11**, 669–671.

Thiesset, F., Antonia, R. A. & Djenidi, L. 2014 Consequences of self-preservation on the axis of a turbulent round jet. *J. Fluid Mech.* **748** (R2).

Van Atta, C. W. & Antonia, R. A. 1980 Reynolds number dependence of skewness and flatness factors of turbulent velocity derivatives. *Phys. Fluids* **23**, 252–257.

Wyngaard, J. C. & Tennekes, H. 1970 Measurements of the small-scale structure of turbulence at moderate Reynolds numbers. *J. Fluid Mech.* **13**, 1962–1969.

Yeung, P. K. & Zhou, Y. 1997 Universality of the Kolmogorov constant in numerical simulations of turbulence. *Phys. Rev. E* **56**, 1746–1752.

Yoffe, S.R. 2012 *Investigation of the transfer and dissipation of energy in isotropic turbulence.* Ph.D. thesis, University of Edinburgh, http://arxiv.org/pdf/1306.3408v1.pdf.

Zhou, T. & Antonia, R. A. 2000 Reynolds number dependence of the small-scale structure of grid turbulence. *J. Fluid Mech.* **406**, 81–107.

Zhou, T., Antonia, R. A. & Chua, L. P. 2005 Flow and Reynolds number dependencies of one-dimensional vorticity fluctuations. *J. Turb.* **6**, 1–17.